



HAL
open science

Simultaneous FAST and Double Star TC1 observations of broadband electrons during a storm time substorm

A. Nakajima, K. Shiokawa, K. Seki, R. Nakamura, K. Keika, W. Baumjohann, T. Takada, J. P. Mcfadden, C. W. Carlson, A. Fazakerley, et al.

► To cite this version:

A. Nakajima, K. Shiokawa, K. Seki, R. Nakamura, K. Keika, et al.. Simultaneous FAST and Double Star TC1 observations of broadband electrons during a storm time substorm. *Journal of Geophysical Research Space Physics*, 2010, 115, pp.7217. 10.1029/2009JA014907 . hal-01553771

HAL Id: hal-01553771

<https://hal.science/hal-01553771>

Submitted on 21 May 2021

HAL is a multi-disciplinary open access archive for the deposit and dissemination of scientific research documents, whether they are published or not. The documents may come from teaching and research institutions in France or abroad, or from public or private research centers.

L'archive ouverte pluridisciplinaire **HAL**, est destinée au dépôt et à la diffusion de documents scientifiques de niveau recherche, publiés ou non, émanant des établissements d'enseignement et de recherche français ou étrangers, des laboratoires publics ou privés.



Simultaneous FAST and Double Star TC1 observations of broadband electrons during a storm time substorm

A. Nakajima,¹ K. Shiokawa,¹ K. Seki,¹ R. Nakamura,² K. Keika,^{2,3} W. Baumjohann,² T. Takada,⁴ J. P. McFadden,⁵ C. W. Carlson,⁵ A. N. Fazakerley,⁶ H. Rème,⁷ I. Dandouras,⁷ R. J. Strangeway,⁸ O. Le Contel,⁹ N. Cornilleau-Wehrin,⁹ and K. H. Yearby¹⁰

Received 17 September 2009; revised 25 January 2010; accepted 4 February 2010; published 21 July 2010.

[1] Broadband electrons (BBEs) exhibit remarkable electron flux enhancements over a broad energy range (0.03–30 keV) near the equatorward edge of the auroral oval during geomagnetic storms. Here, we report a BBE event observed by the Fast Auroral Snapshot (FAST) satellite at 1355–1359 UT, $\sim 61^\circ$ – 66° invariant latitudes, ~ 0600 magnetic local time (MLT), and ~ 3800 km altitude during a storm on 25 July 2004. The Double Star (DS) TC1 satellite was located near the magnetic equator at $L = 5.7$, close to the same local time as FAST. We investigate the acceleration process of BBEs from the inner magnetosphere to near the ionosphere by comparing electron data obtained by FAST and DS TC1. We also investigate both plasma and field variations in the inner magnetosphere associated with substorm onset using DS TC1 data to examine the relationship between the BBEs and the storm time substorm. Ground geomagnetic field data show a positive H-bay at ~ 1349 UT at ~ 0600 MLT, indicating that a storm time substorm started just before the appearance of the BBEs. At ~ 1350 UT, a tailward ion flow was observed by DS TC1. Then, DS TC1 observed a local dipolarization and a drastic ion density enhancement at ~ 1351 UT, indicating that particle heating associated with the substorm was occurring in the inner magnetosphere. From ~ 1352 UT, electron fluxes were isotropically enhanced at energies above ~ 0.5 keV as observed by DS TC1. On the other hand, the pitch angle distribution of BBEs at the FAST altitude showed field-aligned lower-energy electrons below ~ 0.5 keV and isotropic higher-energy electrons above ~ 0.5 keV. From these data, it was inferred that the BBEs might consist of two energy components due to the acceleration or heating of electrons at different altitudes in association with the storm time substorm.

Citation: Nakajima, A., et al. (2010), Simultaneous FAST and Double Star TC1 observations of broadband electrons during a storm time substorm, *J. Geophys. Res.*, 115, A07217, doi:10.1029/2009JA014907.

1. Introduction

[2] Since the early 1970s, auroral electrons have been investigated by many researchers through analyses of electron energy spectra obtained by rockets and ionospheric satellites [e.g., Frank and Ackerson, 1971; Lui et al., 1977; Bryant et al., 1978; McEwen et al., 1981]. The electron energy spectra provide much useful information for under-

standing the acceleration and heating of these electrons. Several studies have shown the characteristics of electron energy spectra, especially during geomagnetic storms [e.g., Denig and Rich, 1986; Egeland et al., 1994; Sharber et al., 1998; Dombek et al., 2005]. However, the spectral characteristics of storm time auroral electrons are still not completely understood owing to the complexity of storm time spectra.

¹Solar-Terrestrial Environment Laboratory, Nagoya University, Nagoya, Japan.

²Space Research Institute, Austrian Academy of Sciences, Graz, Austria.

³Now at Center for Solar-Terrestrial Research, New Jersey Institute of Technology, Newark, New Jersey, USA.

⁴Institute of Space and Astronautical Science, JAXA, Sagami-hara, Japan.

⁵Space Sciences Laboratory, University of California, Berkeley, California, USA.

⁶Mullard Space Science Laboratory, University College London, Dorking, UK.

⁷Centre d'Etude Spatiale des Rayonnements, Toulouse University, CNRS, Toulouse, France.

⁸Institute of Geophysics and Planetary Physics, University of California, Los Angeles, California, USA.

⁹Laboratoire de Physique des Plasmas, Ecole Polytechnique, UPMC, CNRS, Palaiseau, France.

¹⁰Department of ACSE, University of Sheffield, Sheffield, UK.

[3] In the present study, we will analyze broadband electrons (BBEs), which are auroral electrons observed during storms with characteristic spectra. The spectra of BBES are very different from the spectra of ordinary plasma sheet electrons. BBES have drastic electron flux enhancements over a broad energy range (0.03–30 keV) at the lower latitude side of the auroral oval during storms, which has been reported by *Shiokawa et al.* [1996] based on particle observations by Defense Meteorological Satellite Program (DMSP) satellites. The pitch angle distribution of electrons obtained by the Fast Auroral Snapshot (FAST) satellite suggests that BBES consist of two energy components (higher and lower energies) due to the acceleration of electrons at different altitudes [*Nakajima et al.*, 2007, 2008]. In these previous studies of BBES, data from low-altitude satellites (DMSP: ~840 km and FAST: ~350–4200 km) were used. *Shiokawa et al.* [1999] reported a BBE event observed by DMSP when the Combined Release and Radiation Effects Satellite (CRRES) was located at high altitude ($L \sim 6$) at the same local time as DMSP. CRRES observed a drastic enhancement of electron flux at energies of 0.1–10 keV, particularly in the field-aligned direction. However, the detailed spectra of the electrons and ions, including their pitch angle distribution and ion moments at CRRES, were not investigated.

[4] A multievent study of BBES using FAST data [*Nakajima et al.*, 2008] found that, while BBES are associated with substorms during large storms (minimum $Dst < -100$ nT), storm time substorms do not always have BBES. This suggests that BBES are rare or short-lived phenomena.

[5] In this paper, we report a BBE event observed during a storm time substorm on 25 July 2004 using FAST and Double Star (DS) TC1 satellite data. When FAST observed the BBES at ~3800 km, DS TC1 was located near the magnetic equator at $L \sim 5.7$. DS TC1 has higher angular resolution and wider energy coverage of electrons and ions than CRRES. The footprints of FAST and DS TC1 are mapped to similar latitudes separated by ~1 h of local time. The simultaneous observations provide a unique opportunity to compare particle features associated with BBES at FAST altitudes, above the ionosphere, with the inner magnetosphere observations from DS TC1. We investigate the acceleration process of BBES from the inner magnetosphere to near the ionosphere by comparing the electron energy spectra and pitch angle distributions obtained by FAST and DS TC1. We also investigate both plasma and field variations in the inner magnetosphere associated with the substorm onset using DS TC1 data to examine the relation between the BBES and the storm time substorm evolution.

2. Observations

2.1. Data Set

[6] The FAST satellite, which was launched on 21 August 1996, has an 83° inclination polar orbit and a perigee/apogee of 350/4200 km. The orbital and spin periods are ~133 min and ~5 s, respectively. The satellite spin axis is nearly normal to the orbital plane [*Carlson et al.*, 1998]. We use data from the Electrostatic Analyzers (ESAs) [*Carlson et al.*, 2001] and the magnetic field instrument [*Elphic et al.*, 2001] on board FAST. The ESAs provide energy spectra and pitch angle distributions of particles in the local magnetic field

every ~0.6 s during the present event. The energy ranges of the ESAs are 4 eV to 32 keV for electrons. We do not discuss the data of electrons at energies below 30 eV, as these low-energy data are strongly affected by variations of satellite potential.

[7] The Double Star program consists of two spacecrafts. The first spacecraft, TC-1, was launched on 29 December 2003 and placed into an equatorial orbit of $580 \times 79,000$ km altitude with a 28° inclination [*Liu et al.*, 2005]. The DS TC1 satellite has a ~27 h orbit and a ~4 s spin period. In this study, we use electron, ion, magnetic field, and wave data from the Plasma Electron and Current Experiment (PEACE) [*Fazakerley et al.*, 2005], Hot Ion Analyzer (HIA) [*Rème et al.*, 2005], Fluxgate Magnetometer (FGM) [*Carr et al.*, 2005], and Spatiotemporal Analysis of Field Fluctuations (STAFF)-Digital Wave-Processing (DWP) experiment [*Cornilleau-Wehrin et al.*, 2005] of DS TC1, respectively. The PEACE instrument measures electrons at energies from ~1 eV to 25 keV in a 180° field of view and 15° resolution in the polar angle. For the azimuthal angle, there are three sweep modes (angular resolutions of 5.7° , 11.3° , and 22.5°). The HIA instrument performs a full 4π steradian scan completed every spin of the spacecraft, giving a full three-dimensional distribution of ions in the energy range from ~5 eV/q to 32 keV/q. STAFF consists of a three-axis search coil magnetometer for measuring magnetic fluctuations at frequencies up to 4 kHz. DWP provides several onboard analysis tools. One of these tools is a complex fast Fourier transform to fully characterize electromagnetic waves in the frequency range of 1 Hz to 4 kHz.

2.2. Overview

[8] Figure 1 shows an energy-time (E-T) spectrogram of field-aligned downward electrons (pitch angle $<15^\circ$) obtained by FAST at 1340–1410 UT on 25 July 2004. Electron energy fluxes are drastically enhanced over a broad energy range (~0.03–30 keV) at lower invariant latitudes (ILATs) of 66° – 61° , as indicated by the horizontal arrow. Such intense electron fluxes over this broad energy range at the lower latitude side of the auroral oval are identified as BBES. The BBES are observed at magnetic local times (MLTs) of ~6.1–6.4 h and an altitude of ~3800 km at ~1355–1359 UT.

[9] To compare the intensity of the fluxes, energy spectra of field-aligned electrons at pitch angles $<15^\circ$ at 1351:06 UT (curve A), 1356:43 UT (curve B), and 1358:12 UT (curve C) are plotted in Figure 2. The times of curves A–C are indicated by the vertical arrows in Figure 1. The time in curve A is selected as an example of higher-latitude precipitation spectra. In curve B during the appearance of BBES, the electron fluxes are much stronger than those at curve A over the whole energy range. Electron fluxes are even more enhanced over the whole energy range in curve C.

[10] Figures 3a and 3b show the locations of FAST, DS TC1, and the geosynchronous GOES 10 satellite at 1340–1400 UT on 25 July 2004 in the X-Y and X-Z planes of the SM coordinates, respectively. At 1356:43 UT, FAST and DS TC1 crossed the field lines indicated by the dashed and dotted lines, respectively. These field lines were calculated using a geomagnetic field model (T96_01) by *Tsyganenko* [1995, 1996].

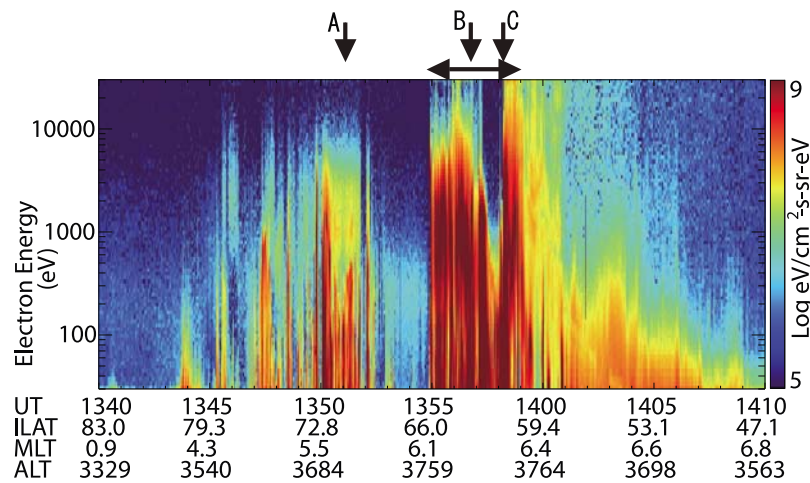


Figure 1. Energy-time (E-T) spectrogram of field-aligned electrons (pitch angle $<15^\circ$) for differential energy flux obtained by FAST at 1340–1410 UT on 25 July 2004. Horizontal arrow indicates time interval of the BBE event identified in this paper. Vertical arrows indicate times (Figure 2, curves A–C) of electron energy spectra.

[11] When FAST passed from the northern pole across the auroral zone and observed the BBES at ~ 1355 – 1359 UT, the three satellites were located nearly in the same local time (~ 0600 MLT) in the Northern Hemisphere. At 1400 UT, the positions of DS TC1 and GOES 10 were (X, Y, Z) $\sim (-2, -5, 1) R_E$ and $\sim (-2, -6, 1) R_E$, respectively. These satellites were near the magnetic equator in the inner magnetosphere. When we later compare FAST and DS TC1 electron data at 1356:43 UT, the footprints of FAST and DS TC1 at the magnetic equator are separated by $\sim 3 R_E$.

[12] In Figure 4, the satellite track of FAST in geographical coordinates at an altitude of 100 km in the Northern Hemisphere is denoted by the solid line with asterisks every 10 min during 1340–1400 UT. This satellite passed from the northern arctic region to lower latitudes. On the other hand, the footprints of DS TC1 and GOES 10 indicated by the open diamond and open circle, respectively, did not move significantly. These footprints were calculated using the T96_01 geomagnetic field model [Tsyganenko, 1995, 1996]. The footprint mapping using the T96_01 model contains uncertainty, because this mapping calculation is strongly influenced by magnetic field variation during storms and substorms. The present BBE event took place during a storm time substorm, as will be shown later. We must keep in mind this uncertainty when comparing observations of FAST and DS TC1. The locations of the ground-based magnetometer and riometer stations, which are shown in Figures 6 and 7 and discussed in section 2.3, are also shown. The top and right of Figure 4 are sunward and downward, respectively.

[13] As shown in Figure 4, the footprints of FAST, DS TC1, and GOES 10 at 1400 UT were at (51°N , 255°E), (54°N , 240°E), and (53°N , 243°E) in the dawnside sector, respectively. These footprints are mapped to similar latitudes with differences of less than 5° during the BBE event. The local time difference between these footprints was less than 1 h. Riometer data indicate that enhanced electron precipitation was occurring throughout the spatial region that included the FAST, GOES, and DS TC1 ionospheric foot-

prints, as will be noted in section 2.6. It is reasonable to speculate that the enhanced electron precipitation over the entire region results from the same mechanisms. In an event study of BBES observed by FAST, Nakajima *et al.* [2007] reported that simultaneous auroral images from the Polar

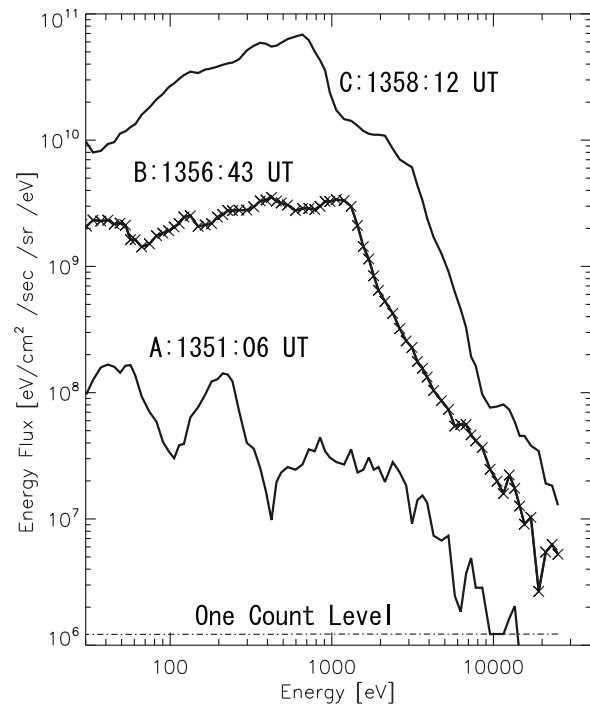


Figure 2. Electron energy spectra of field-aligned electrons (pitch angle $<15^\circ$) obtained by FAST at 1351:06 UT (curve A), 1356:43 UT (curve B), and 1358:12 UT (curve C) on 25 July 2004. Times are indicated by vertical arrows in Figure 1. Crosses on energy spectrum (curve B) indicate energy steps of ESAs, which are almost the same for all three spectra. Dashed-dotted line shows one count level of ESAs.

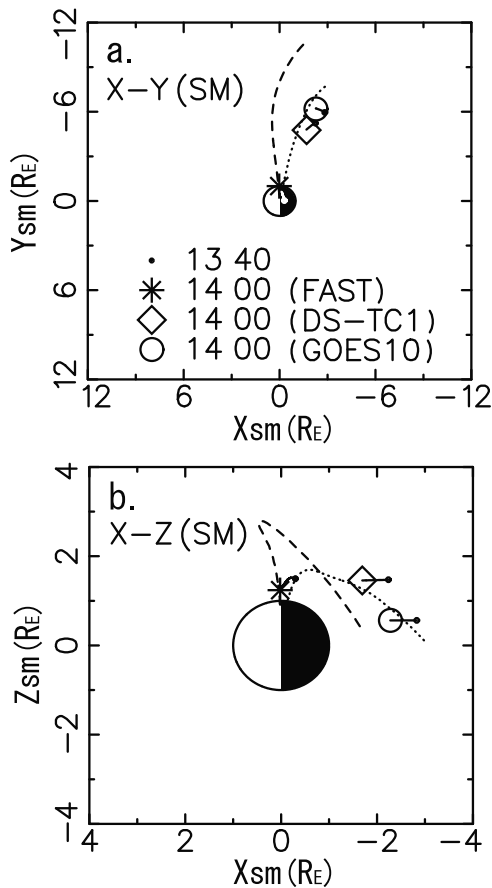


Figure 3. Locations of FAST, DS TC1, and GOES 10 at 1340–1400 UT on 25 July 2004 in (a) X-Y and (b) X-Z planes in SM coordinates. Small solid circles indicate locations of the three satellites at 1340 UT. Asterisk, open diamond, and open circle show the locations of FAST, DS TC1, and GOES 10 at 1400 UT, respectively. At 1356:43 UT, FAST and DS TC1 crossed the magnetic field lines indicated by dashed and dotted lines, respectively. Field lines from ground in the Northern Hemisphere to magnetic equator were calculated using the geomagnetic field model (T96_01) by *Tsyganenko* [1995, 1996].

satellite showed that the precipitating region of BBES covered $\sim 10^\circ$ in latitude and ~ 1 h in local time, which included the ionospheric footprint of FAST.

[14] Figure 5 shows the variation of the *Dst* index on 24–27 July 2004. A large geomagnetic storm started at 0400 UT on 24 July and the *Dst* index reached a minimum value (~ -150 nT) at 1000 UT on 25 July. The BBES reported in this paper were observed around the *Dst* minimum at ~ 1400 UT, as indicated by the vertical arrow.

2.3. Magnetic Field Variations

[15] To clarify the relation of the BBE event to the substorm, we examined the magnetic field data obtained by the geosynchronous GOES 10 satellite and ground-based stations. Figure 6a shows the magnetic field data (time resolution: 1 min) obtained by GOES 10. From the top to bottom in Figure 6a, the X, Y, and Z components of the GSM coordinates at 1200–1500 UT on 25 July 2004 are

plotted. Figure 6b shows geomagnetic H component variations from high- to low-latitude stations. The station names and locations are listed in Table 1. As shown in Figure 4, the footprint of GOES 10 and the ground stations was at ~ 0500 – 0600 MLTs when FAST observed the BBES at ~ 1355 UT.

[16] GOES 10 observed decreasing B_x and increasing B_z beginning at ~ 1347 UT, as indicated by the vertical dotted line in Figure 6a, indicating that dipolarization started at this time. The B_y component temporarily increased in association with the dipolarization. Negative and positive H-bays at higher- and lower-latitude ground stations, respectively, were also observed around this time. We identified starts of positive/negative magnetic field variation as the starts of positive/negative H-bays, which represent substorm onset signatures. The earliest substorm signatures on the ground were at SIM (MLT = 5.0 h) at ~ 1349 UT, as indicated by the dotted line in Figure 6b. A few minutes later, the substorm signatures were detected in other latitudinal regions, for example, at ~ 1350 UT at MEA.

[17] The geomagnetic H and D variations at low latitudes from ~ 1000 to 0300 MLTs are plotted in Figures 7a and 7b, respectively. The station names and locations are shown in Table 1 and Figure 4. At all stations between ~ 1000 and 0500 MLTs, positive H-bays started at ~ 1350 UT, as indicated by the vertical dotted line in Figure 7a, with the exception of HON at ~ 0300 MLT. In Figure 7b, geomagnetic D components began to decrease at ~ 1350 UT between ~ 1000 and 0500 MLTs associated with the H-bays. At HON, however, no notable magnetic field variation was observed at 1350 UT.

2.4. FAST Observation

[18] Figures 8a–8d show electron (0.6 s sampling) and magnetic field (8 Hz sampling) data obtained by FAST at 1354–1400 UT. Electron energy fluxes were drastically enhanced over a broad energy range (~ 0.03 – 30 keV) at ~ 1355 – 1359 UT in the omnidirectional E-T spectrogram (Figure 8a). However, to be exact, the electron fluxes temporarily decreased during 1357:30–1358:00 UT. In Figure 8a, the time interval of the BBE event is precisely indicated by the horizontal arrows. Figures 8b and 8c show the pitch angle distributions of electrons at energies below and above 0.5 keV, respectively.

[19] During the BBE event, field-aligned downward fluxes ($\sim 0^\circ$) were most intense at energies below 0.5 keV, as shown in Figure 8b. Field-aligned upward fluxes ($\sim 180^\circ$) were sometimes enhanced (e.g., at $\sim 1357:10$ UT). On the other hand, electron fluxes above 0.5 keV tended to be more isotropic (Figure 8c), although the field-aligned downward fluxes were slightly larger than the fluxes in other directions. The reduced upward energy flux has features of the loss cone.

[20] Figure 8d shows the three-component magnetic field variations in the field-aligned coordinate system. The blue curve indicates the magnetic field variations along the local magnetic field given by the International Geomagnetic Reference Field (IGRF) model. The red and green curves are the magnetic fields along the spacecraft velocity vector (nearly north–south) and in the nearly east–west direction, respectively.

[21] The magnitudes of magnetic field variations during the BBE event are larger than those at the higher-latitude

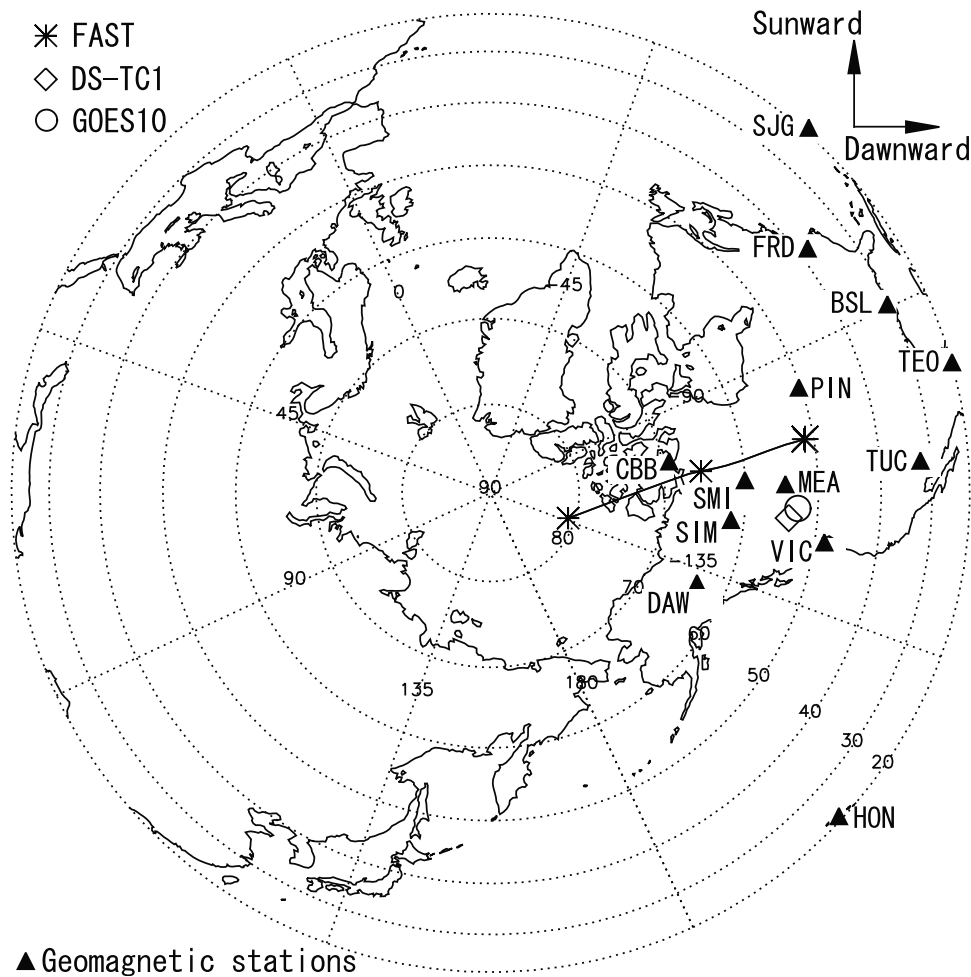


Figure 4. Satellite track of FAST at altitude of 100 km in the Northern Hemisphere in geographical coordinates is shown by a solid line with an asterisk denoting every 10 min during 1340–1400 UT. During this time, footprints of DS TC1 and GOES 10 indicated by the open diamond and open circle, respectively, were located at almost the same latitude and longitude. These footprints were calculated using the T96_01 geomagnetic field model [Tsyganenko, 1995, 1996]. Closed triangles indicate ground-based magnetometer and riometer stations, which are used in Figures 6 and 7 and section 3.

region above $\sim 66^\circ$ ILAT (Figure 8d). Intense fluctuations of the magnetic field were occasionally observed in the north–south and east–west magnetic fields (e.g., $\sim 1357:10$ UT).

[22] We compared the current density of the field-aligned current (FAC) estimated from the electron and magnetic field data in Figures 8e and 8f, respectively. Both methods of estimating the FAC have uncertainties. The electron ESA can provide a current density estimated from a measurement of the number flux; however, since the energy range of ESA is limited, lower energy electrons that can carry significant current density are not included in the estimated current density. This usually affects the calculation of downward current densities, which are carried by upward flowing electrons. The FAC density is also calculated by taking the gradient of the magnetic field along the spacecraft trajectory. This implicitly assumes that the FAC is an infinite sheet current, oriented perpendicular to the spacecraft trajectory. It is further assumed that the current sheet is stationary in time and space.

[23] Despite the above mentioned observational limits of the ESA and the assumptions made to estimate the FAC, the current densities estimated by the two methods have significant similarities, as shown in Figures 8e and 8f. The agreement is not perfect, but good agreement can be seen in the variation and intensity of current density between 1357:00 and 1357:20 UT when the electron energy flux is especially intense during the BBE event. These similarities during the time interval plotted in Figures 8e and 8f indicate that precipitating electrons over the measurable energy range of ESA play a major role as carriers of the FAC. The spatial structure of the FAC possibly appears as magnetic field variation. Based on this result, the FAC can be regarded as an almost stationary sheet current in time and space when observed by satellite. This result indicates that BBES possibly correspond to a complex region of both upward and downward currents rather than a uniform upward current region, although BBES are an intense precipitation of electrons.

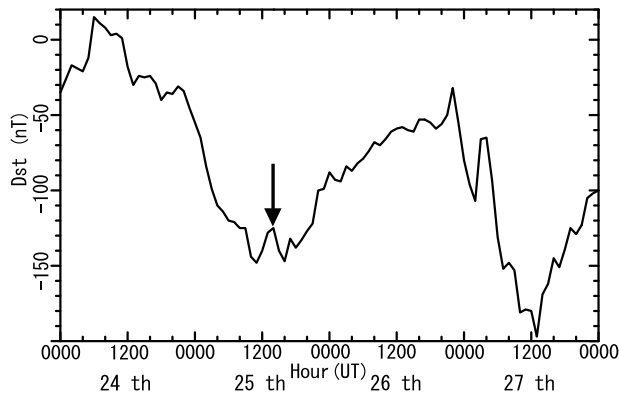


Figure 5. *Dst* index on 24–27 July 2004. Vertical arrow indicates time when BBES were observed by FAST.

2.5. DS TC1 Observation

[24] Figure 9 shows magnetic field, electron, ion, and wave data at 1340–1400 UT obtained by the FGM, PEACE, HIA, and STAFF-DWP onboard DS TC1, respectively. The

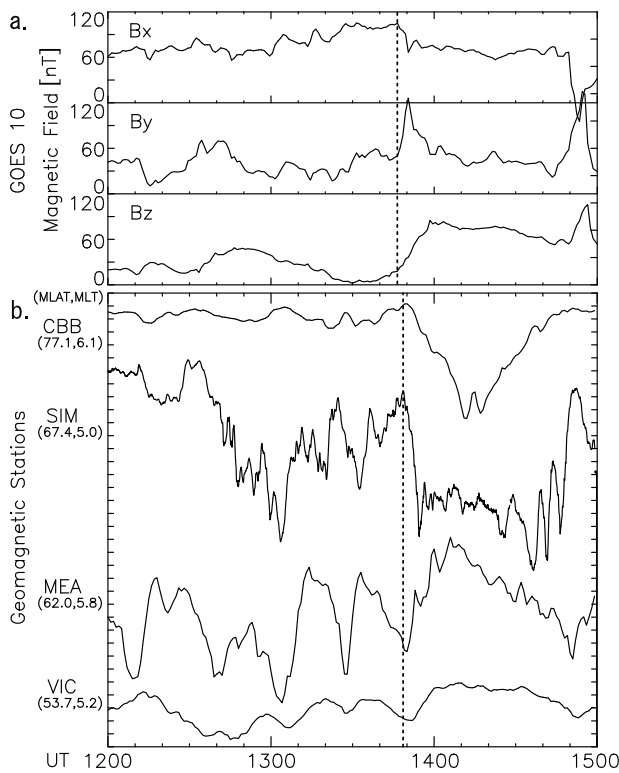


Figure 6. (a) X, Y, and Z components of magnetic field in GSM coordinates obtained by GOES 10 and (b) H component of magnetic fields at ground-based stations at 1200–1500 UT on 25 July 2004. In Figure 6b, data are shown from top to bottom in descending order of geomagnetic latitudes. GOES 10 and all stations are around the same local time as BBES (~0600 MLT), as shown in Figure 4. Higher-latitude (CBB, SIM, and MEA) and lower-latitude (VIC) station data are plotted in 100 and 40 nT/div, respectively. Station names and locations are listed in Table 1. Vertical dotted lines in Figures 6a and 6b denote 1347 and 1349 UT, respectively.

Table 1. Ground-Based Geomagnetic Stations Shown in Figures 6 and 7^a

Station	Abbreviation	GLAT	GLONG	MLAT
Bay St. Louis	BSL	30.4°N	270.4°E	41.2°N
Cambridge Bay	CBB	69.1°N	255.0°E	77.1°N
Fort Simpson	SIM	61.8°N	238.8°E	67.4°N
Fredericksburg	FRD	38.2°N	282.6°E	48.9°N
Honolulu	HON	21.3°N	202.0°E	29.2°N
Meanook	MEA	54.6°N	246.7°E	62.0°N
San Juan	SJG	18.1°N	293.9°E	27.5°N
Teoloyucan	TEO	19.7°N	260.8°E	29.2°N
Tucson	TUC	32.2°N	249.3°E	39.8°N
Victoria	VIC	48.5°N	236.6°E	53.7°N

^aGLAT, geographic latitude; GLONG, geographic longitude; MLAT, dipole geomagnetic latitude.

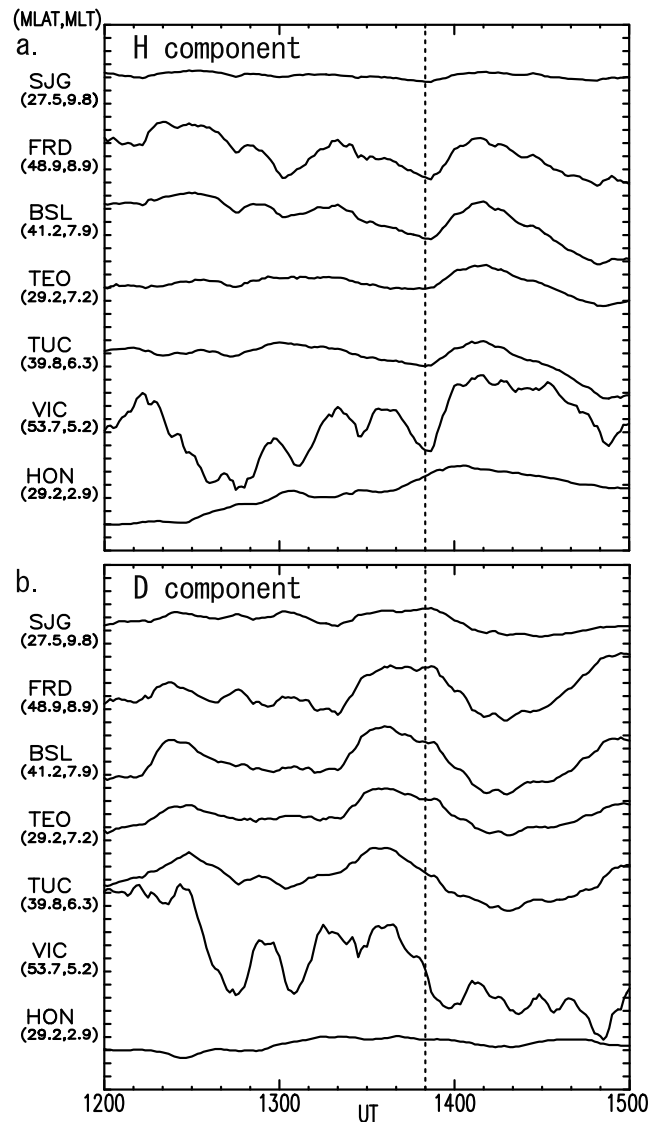


Figure 7. Geomagnetic (a) H and (b) D components observed at ground-based stations at 1200–1500 UT on 25 July 2004. From top to bottom in Figures 7a and 7b, data are shown from ~1000 to ~0300 MLTs, all of which are at latitudes below 55° MLAT. Data are plotted at 20 nT/div. Station names and locations are shown in Table 1 and Figure 4. Vertical dotted lines indicate 1350 UT.

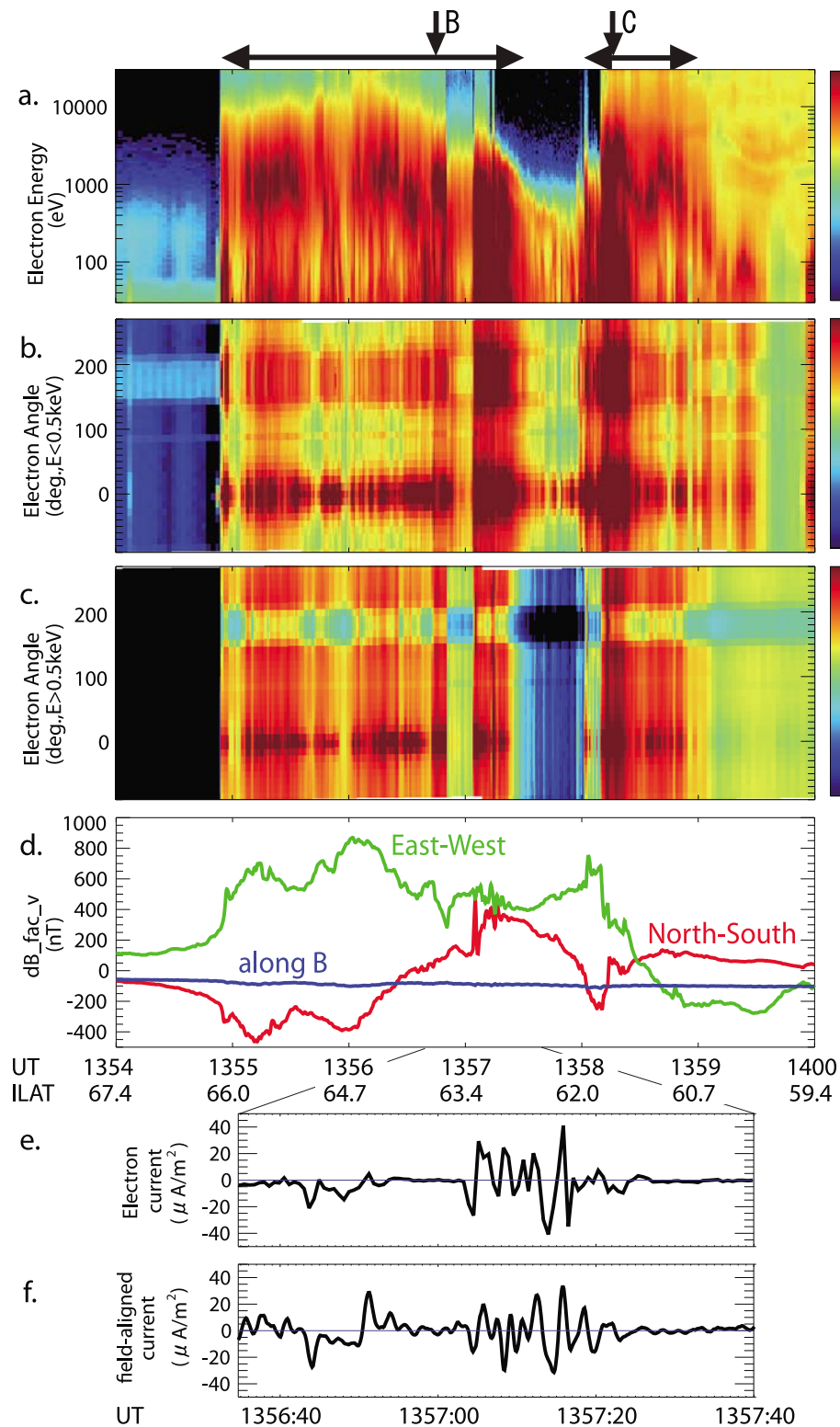


Figure 8. (a) Omnidirectional E-T spectrogram and pitch angle distributions (0° is field-aligned downward) of electrons at energy ranges (b) below and (c) above 0.5 keV, (d) three-component magnetic field in field-aligned coordinate system (blue, field-aligned component; red, nearly north–south component; green, nearly east–west component) observed by FAST at 1354–1400 UT on 25 July 2004. Current densities of FAC estimated from (e) electron number flux and (f) gradient of the magnetic field at 1356:35–1357:40 UT. Horizontal arrows indicate time intervals of the BBE events. Vertical arrows denote times at which pitch angle distributions and energy spectra of FAST in Figures 10 and 11 were obtained.

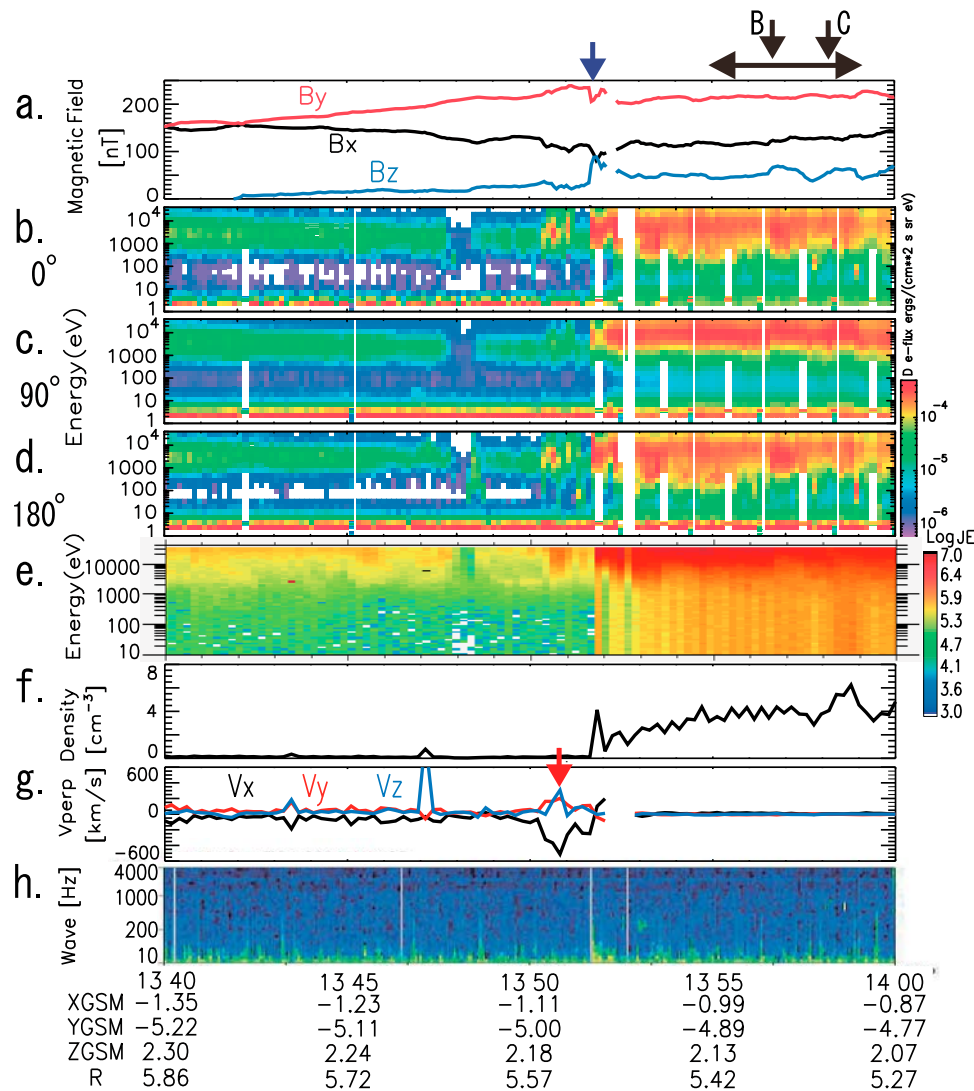


Figure 9. (a) Magnetic field, E-T spectrograms of (b) field-aligned downward, (c) perpendicular, and (d) upward electrons, (e) omnidirectional E-T spectrogram of ions, (f) ion density, (g) perpendicular ion velocities, and (h) wave spectrogram of magnetic field between 10 and 4000 Hz obtained by DS TC1 at 1340–1400 UT on 25 July 2004. For magnetic field and ion velocity in Figures 9a and 9g, X, Y, and Z components in GSM coordinates are indicated by black, red, and blue curves, respectively. Horizontal arrows indicate time periods when BBES were observed by FAST. Black vertical arrows show times at which pitch angle distributions and energy spectra of DS TC1 in Figures 10 and 11, respectively, were obtained. Times of local dipolarization in Figure 9a and intense tailward ion flux in Figure 9g are indicated by blue and red vertical arrows, respectively.

horizontal arrow in Figure 9a indicates the time period when BBES were observed by FAST. In Figure 9a, the black, red, and blue curves indicate the X, Y, and Z components of the magnetic field in the GSM coordinates, respectively. The time resolution of the data is ~ 4 s, which is the spin period of DS TC1. Figures 9b–9d show E-T spectrograms of field-aligned downward, perpendicular, and upward electrons, respectively. The electron-energy spectra in Figures 9b–9d were calculated once per spin (~ 4 s). Figures 9e–9g show omnidirectional E-T spectrograms of ions, ion density, and ion velocity, respectively. The ion spectra in the E-T spectrograms and ion moment data (density and velocity) were

calculated every three spins (~ 12 s). In Figure 9g, the black, red, and blue curves indicate the ion velocities in the X, Y, and Z directions in GSM coordinates, respectively. Figure 9h shows the magnetic field wave spectrogram between 10 and 4000 Hz. This spectrogram was obtained by combining the signals from the three axes of the STAFF antenna to simulate a single axis oriented to minimize interference. The time resolution of this spectrogram is ~ 4 s. The frequency scale of the spectrogram is linear below 200 Hz and approximately logarithmic above that.

[25] In Figure 9g, we plotted ion velocities perpendicular to the local magnetic field, which were calculated from the

ion velocity data, $\mathbf{V} = (V_x, V_y, V_z)$, and magnetic field data, $\mathbf{B} = (B_x, B_y, B_z)$, obtained by DS TC1. The field-aligned ion velocity, $\mathbf{V}_{\parallel} = (V_{\parallel x}, V_{\parallel y}, V_{\parallel z})$, is defined as $\mathbf{V}_{\parallel} = (\mathbf{b} \cdot \mathbf{V}) \mathbf{b}$, where $\mathbf{b} = (b_x, b_y, b_z)$ is the unit vector of the magnetic field. From $\mathbf{V} = \mathbf{V}_{\parallel} + \mathbf{V}_{\perp}$, three components of the perpendicular ion velocity, $\mathbf{V}_{\perp} = (V_{\perp x}, V_{\perp y}, V_{\perp z})$, are estimated.

[26] We should note that oscillating noise in the HIA instrument is observed over the entire energy range in the E-T spectrogram of ions, particularly at 1351–1400 UT, in Figure 9e. In Figures 9f and 9g, this noise causes some oscillations in the ion moment data on a timescale comparable to the data resolution (~ 12 s). We only discuss variations of the ion moments with amplitudes larger than the noise.

[27] In Figure 9a, local dipolarization (decreasing B_x and increasing B_z) was observed at $\sim 1351:30$ UT, as indicated by the blue vertical arrow. In association with the dipolarization, B_y temporarily decreased. This dipolarization was observed ~ 4 min after that observed by GOES 10 at $L = 6.6$ which was further from the earth than DS TC1 at $L = 5.7$.

[28] Immediately after $\sim 1351:30$ UT, electron and ion fluxes nearly simultaneously intensified at all energies monitored with PEACE and HIA (Figures 9b–9e). In association with the flux intensification, ion density was enhanced at ~ 1351 – 1400 UT (Figure 9f). Wave power over a broad frequency range of 10–200 Hz (Figure 9h) and at lower frequencies of 1–10 Hz (not shown) was enhanced temporarily at $\sim 1351:30$ UT.

[29] The magnetic reconnection site at substorm expansion onset is usually located at $-20 > X > -30 R_E$ [e.g., Baumjohann *et al.*, 1989, 1999; Nagai *et al.*, 1998; Miyashita *et al.*, 2000, 2003]. At radial distances earthward of the reconnection site in the tail plasma sheet, earthward ion flow perpendicular to the local magnetic field is usually observed in association with the substorm onset. However, such earthward flow was not observed by DS TC1 during the present event. On the other hand, DS TC1 observed intense perpendicular tailward flow at $\sim 1350:25$ – $1351:40$ UT (beginning ~ 1 min before the local dipolarization) (Figure 9g). At 1350:50 UT, as indicated by the red vertical arrow in Figure 9g, the tailward, duskward, and northward perpendicular ion velocity of $(V_x, V_y, V_z) \sim (-500, 200, 300)$ km/s was observed by DS TC1 at $L \sim 5.7$, though these absolute values are affected by the noise in the HIA data. However, the fluctuation of the ion velocity is larger than that of the noise. We also confirmed the reliability of ion velocity by monitoring the distribution function around this time interval. This perpendicular flow burst at the substorm onset will be discussed in section 3.

2.6. Comparison of Electron Data of FAST and DS TC1

[30] While the electron flux enhancement was observed by DS TC1 at ~ 1351 – 1400 UT in Figures 9b–9d, the BBES were observed by FAST at 1355–1359 UT, as shown in Figure 8a. In Figure 10, we compare the pitch angle distributions of electrons observed by FAST (Figure 10, top) and DS TC1 (Figure 10, bottom) simultaneously at (B) 1356:43 UT (Figure 10, left) and (C) 1358:12 UT (Figure 10, right) on 25 July 2004. These times are indicated by the vertical black arrows in Figures 8 and 9. These pitch angle distributions were obtained by FAST and DS TC1 every ~ 1 s and ~ 8 s, respectively.

[31] Based on the T96_01 model, the latitudinal separations between the footprints of these satellites are 0.4° (at (B) 1356:43 UT) and 3° (at (C) 1358:12 UT) in geographic latitude (3° and 5° in geomagnetic latitude (MLAT)), while the local time separation is ~ 1 h for both events.

[32] Footprint mapping using the T96_01 model contains uncertainty, as noted in section 2.2. In particular, variation in the global magnetic field during substorms and storms affects this mapping calculation. For the footprint calculation, we used the observed value for the Dst index of -125 nT and the interplanetary magnetic field along the north–south direction (IMF- B_z) of -14 nT in the T96_01 model. We also checked the variation in the footprint for $Dst = 0, -50, -100,$ and -150 nT and IMF- $B_z = -5, -10,$ and -20 nT. The variation of DS TC1 footprint was $< 5^\circ$ in latitude and $< 1^\circ$ in longitude, and that of FAST was $< 0.2^\circ$ in latitude and $< 1^\circ$ in longitude for these changes in Dst and IMF- B_z .

[33] We also examined riometer data (not shown) obtained in the Canadian sector near the footprints of the FAST and DS TC1 satellites during the present BBE event. The absorptions intensified during 1350–1420 UT at Dawson (DAW, 65.9° MLAT, 3.3 MLT), Fort Smith (SMI, 67.5° , 5.7 MLT), and Pinawa (PIN, 60.3° , 7.2 MLT) compared with those at 1330 UT. The locations of these stations are plotted in Figure 4. These results indicate that the footprints of both FAST and DS TC1 were located in the enhanced electron precipitation region. It therefore seems reasonable to assume that, even though the satellite footprints are separated, they lie within the same precipitation region, and so are observing the signatures of the acceleration processes on essentially the same flux tubes.

[34] From FAST data at (B) 1356:43 UT in Figure 10 (top left), field-aligned electron fluxes were most intense, and perpendicular fluxes were weakest at lower energies below ~ 0.5 keV. In contrast, at higher energies above ~ 0.5 keV, electron fluxes were isotropically enhanced with an upward loss cone. Similar pitch angle features at lower and higher energies for FAST data were seen also at (C) 1358:12 UT, as shown in Figure 10 (top right), although the flux intensities over all energies were more intense at (C) 1358:12 UT than those at (B) 1356:43 UT. In Figure 10 (bottom), the electron fluxes were isotropic at energies above ~ 0.5 keV at DS TC1 at both (B) 1356:43 UT and (C) 1358:12 UT. Field-aligned low-energy electrons observed by FAST were not observed by DS TC1. Similar pitch angle characteristics were continuously observed during ~ 1355 – 1359 UT at FAST in Figures 8b and 8c and during ~ 1353 – 1400 UT at DS TC1 in Figures 9b–9d, respectively.

[35] We also compare electron energy spectra obtained by FAST and DS TC1 at (B) 1356:43 UT in Figure 11. The solid and dotted curves show energy spectra of field-aligned downward and perpendicular electrons obtained by FAST. The energy spectrum of field-aligned downward electrons obtained by DS TC1 is indicated by the dashed curve. As can be seen in Figure 10, the energy spectrum obtained by DS TC1 exhibited flux enhancement mainly at higher energies above ~ 0.1 keV. On the other hand, the spectrum of field-aligned electrons obtained by FAST showed flux enhancements at energies not only above ~ 0.5 keV but also below ~ 0.5 keV. The shape of the spectrum obtained by DS TC1 had a moderately energetic peak of a few keV, which

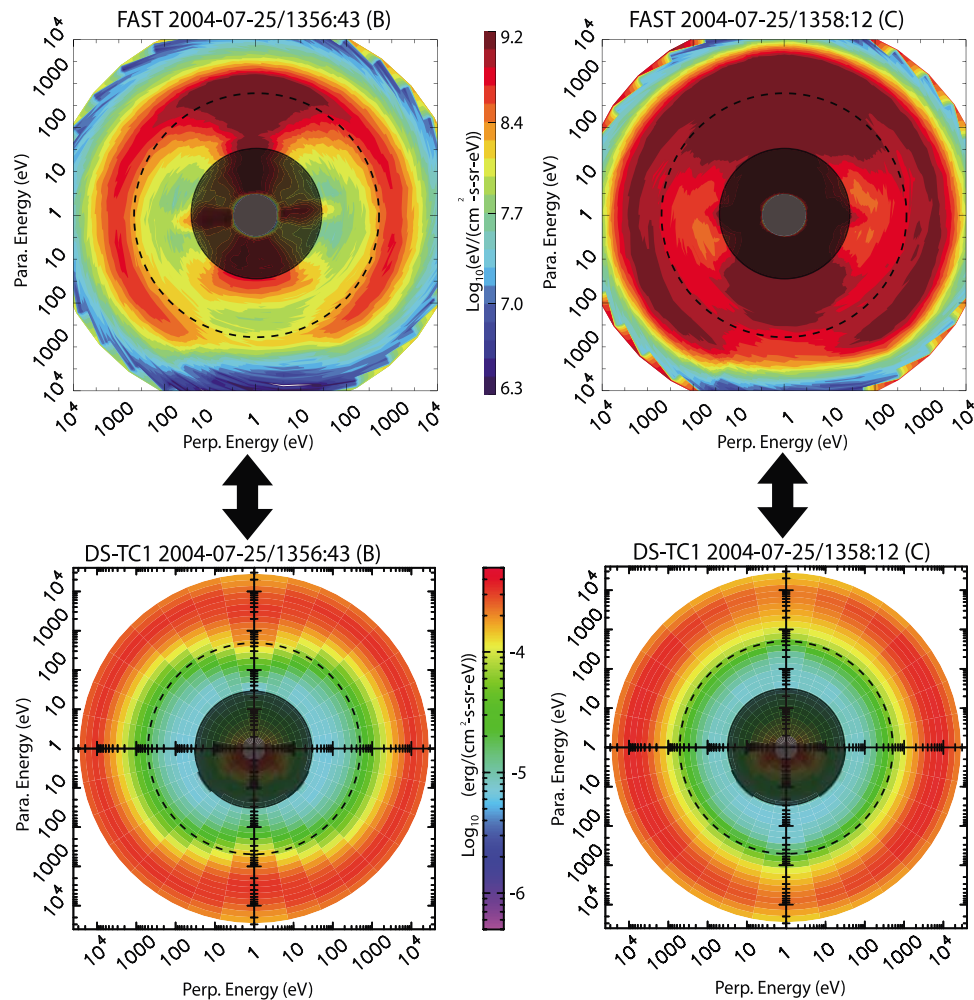


Figure 10. Pitch angle distributions using differential electron energy flux as functions of energy and pitch angle obtained by (top) FAST and (bottom) DS TC1 at (left) 1356:43 UT and (right) 1358:12 UT on 25 July 2004. These times are indicated by vertical black arrows in Figures 8 and 9. Upper sides of vertical axes and horizontal axes indicate field-aligned downward (0°) and perpendicular directions, respectively. Dashed circle in each plot indicates energy of 0.5 keV. Lower-energy electron data (<30 eV) are hidden by black disks, as these data are not discussed and are possibly affected by variations of satellite potential. Note that units of differential electron energy flux are different between these satellite data.

was similar to that of perpendicular electrons obtained by FAST at energies above 0.1 keV.

3. Discussion

3.1. Relation to Storm Time Substorm

[36] Previous studies have shown that BBES mostly appear during substorms in the main phase of geomagnetic storms [e.g., *Shiokawa et al.*, 1997]. *Baumjohann et al.* [1996] reported a clear difference in the dynamics of the near-Earth tail for substorms that occur during the main phase of storms and for non-storm time substorms. The magnetic field dipolarization and the earthward convection in the near-Earth tail are much more pronounced for substorms during the main phase of storms than for nonstorm substorms. *Schödel et al.* [2002] concluded that the transport of plasma and of magnetic flux is greatly enhanced during the main phase of the storm. It is difficult to understand

substorm processes that occur during magnetic storms owing to complex plasma and field evolution in the inner magnetosphere. This study and related researches on BBES can aid us in understanding the complex plasma dynamics in the inner magnetosphere during storm time substorms.

[37] The BBES presented in this paper occurred during the main phase of a large storm at ~ 0600 MLT. During the appearance of BBES, both DS TC1 and GOES 10 were located near the dawnside magnetic equator. Footprints of FAST, DS TC1, and GOES 10 were mapped to similar latitudes with differences of less than 5° and local time separation of ~ 1 h during the BBES event. At ~ 1347 UT, GOES 10 observed dipolarization on the geosynchronous orbit ($L = \sim 6.6$). Positive and negative H-bays were observed by the ground-based stations at ~ 0500 – 0600 MLTs at ~ 1349 UT. Around this time, magnetic Pi 2 pulsations were also observed at low-latitude stations (e.g., HON at 2.9 MLT) (data not shown). DS TC1 observed a local

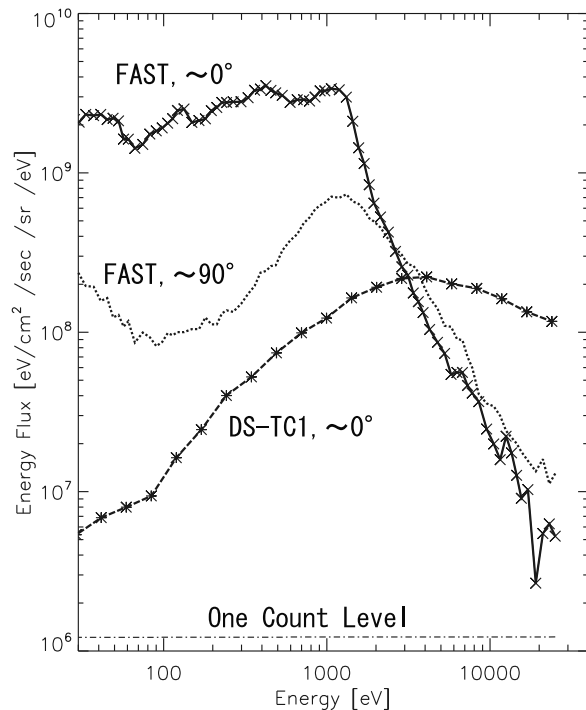


Figure 11. Solid and dotted curves show energy spectra of field-aligned downward (pitch angle within 15°) and perpendicular (pitch angle between 75° and 105°) electrons observed by FAST at 1356:43 UT on 25 July 2004 (Figure 10, top left). Dashed curve indicates spectrum of field-aligned electrons obtained by DS TC1 at 1356:43 UT (Figure 10, bottom right). Time of Figures 10 (top left) and 10 (bottom right) is indicated by the vertical black arrows in Figures 8 and 9. Crosses on the solid curve and asterisks on the dashed curve denote energy steps for ESAs of FAST and PEACE of DS TC1, respectively.

dipolarization at $L \sim 5.7$ at ~ 1351 UT. These facts indicate that a substorm began at ~ 0500 – 0600 MLTs at 1347–1349 UT. The BBES occurred in association with the storm time substorm, which has been reported in previous studies of BBES using the magnetic field data obtained in the geosynchronous orbit and on the ground [Shiokawa *et al.*, 1996; Nakajima *et al.*, 2007, 2008]. In this study, we examined the

plasma dynamics in the inner magnetosphere associated with the storm time substorm by using data obtained by DS TC1.

[38] Since the average location of the magnetic reconnection site is $-20 > X > -30 R_E$ at substorm expansion onset [e.g., Baumjohann *et al.*, 1989, 1999; Nagai *et al.*, 1998; Miyashita *et al.*, 2000, 2003], earthward ion flow is usually observed at the near-Earth magnetotail. The location of the reconnection site appears to be much closer to the Earth during geomagnetic storms than the location reported in previous studies. Miyashita *et al.* [2005] suggested that the reconnection occurred earthward of $X \sim -8.6 R_E$ during a large storm (minimum $Dst \sim -400$ nT) on 30 October 2003, based on observations by the Geotail satellite. On the other hand, Takada *et al.* [2006] examined the relationship between bursty bulk flow events (> 300 km/s) observed by the Cluster satellites between $-19 < X < -12 R_E$ and dipolarization events observed by DS TC1 between $-13 < X < -6 R_E$, based on conjunction events in the nightside magnetotail ($|Y| < 10 R_E$) in summer 2004. They found no evidence of a fast flow event associated with dipolarization when DS TC1 was at $X > -8 R_E$.

[39] For the present event, however, DS TC1 at $L \sim 5.7$ observed intense tailward ion flux at $\sim 1350:25$ – $1351:40$ UT, which was just after the substorm onset. Considering the above mentioned previous works, the intense tailward ion flux at $L \sim 5.7$ is somewhat unusual, although the present case is on the dawnside rather than nightside. The only theoretically viable explanation available at this time is that the perpendicular tailward ion flux at the onset was caused by combination of a steep density gradient near the spacecraft with the finite gyroradius effect of high-energy ions, as discussed by Ohtani *et al.* [2000, Figure 1].

[40] When the most intense tailward ion flow was detected by DS TC1 at $(X, Y, Z) \sim (-1, -5, 2) R_E$ at 1350:50 UT, the perpendicular ion velocity components were $(V_x, V_y, V_z) \sim (-500, 200, 300)$ km/s. The magnetic field intensity was $(B_x, B_y, B_z) \sim (110, 230, 30)$ nT. In order to explain the observed tailward perpendicular ion flux, based on the ion motion with finite gyroradius and the direction of the magnetic field observed by DS TC1, we consider that the high ion density region appeared inside DS TC1 as shown in Figure 12. In this situation, due to the equatorward ion density gradient at the dawnside in the inner magnetosphere, the tailward ion flux from the high-

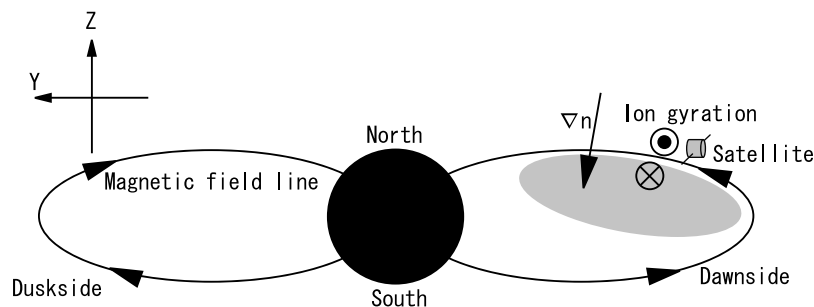


Figure 12. Schematics of satellite positions, magnetic field configuration, and expected density gradient of ions in the Y - Z plane of GSM coordinates. Directions of ion gyration are indicated by the circles with the cross (inward) and the dot (outward). Shaded regions indicate areas thought to have high ion population based on DS TC1 observations.

density region associated with the ion gyration motion was more intense than the earthward flux of the gyration. Similarly, the duskward and northward ion flux could be interpreted in terms of the equatorward and tailward ion density gradients.

[41] We examined the pitch angle distribution of ions to verify the possibility of nonisotropic ion gyration due to the density gradient. During the time interval when the tailward flux was observed at $\sim 1350:25$ – $1351:40$ UT, the pitch angle distribution was sometimes not isotropic in the plane perpendicular to the local magnetic field (e.g., at $1350:55$ UT), although such a feature was not continuously observed and the flux decreased below a detectable level (e.g., at $1350:43$ UT). Ion density enhancement was observed by DS TC1 just after these perpendicular ion flows, implying that the expected region of high ion population expanded outward to the DS TC1 location. From ~ 1352 UT, DS TC1 observed isotropic and drastic enhancements of the electron and ion fluxes at energies above ~ 0.5 keV, which continued until 1400 UT for the rest of the plotted interval in Figures 9b–9e. We conclude that heating of particles was occurring in the inner magnetosphere just after the substorm onset and possibly generated the high-population region of ions in the equatorward and tailward region of DS TC1.

[42] Accompanied by the ion density enhancement at ~ 1351 UT, DS TC1 temporarily observed an enhancement of the magnetic wave or magnetic field fluctuations over a broad frequency range of ~ 1 – 200 Hz. Since such an enhanced wave was not continuously observed during the particle flux enhancement region from ~ 1352 UT, the wave might not contribute to acceleration or heating of the observed high-energy particles. The waves are perhaps enhanced at the boundary of the expected high-population region of ions.

[43] Geomagnetic H-bay was first observed at ground-based stations located at ~ 0500 MLT (SIM) at 1349 UT. At nearly the same time, positive H-bays were seen at ground stations at 0500–1000 MLTs. The D components at the stations of 0500–1000 MLTs started to decrease at ~ 1350 UT in association with the H-bays. On the other hand, at ~ 0300 MLT station (HON), notable magnetic field variations of the H and D components were not observed at ~ 1350 UT. Furthermore, at ground stations at 2100–0200 MLTs, no pronounced magnetic field variations were observed 10 min before and after 1350 UT, although we investigated ground magnetic field data at other local times including nightside (not shown). From the ground magnetometer data, we speculate that FAST observed a downward field-aligned current that was generated at substorm onset. On 25 July 2004, an intense negative Y component of IMF between -5 nT and -18 nT lasted 8.5 h from 0620 to 1450 UT. It would appear that this large negative IMF B_y was related to the dawnside onset of the substorm.

3.2. Generation Mechanism

[44] The pitch angle distributions of BBES at the FAST altitude had isotropic features at high energies above ~ 0.5 keV with an upward loss cone, while below ~ 0.5 keV field-aligned electron fluxes were most intense. These observations were consistent with the statistical characteristics of the pitch angle of BBES reported by Nakajima *et al.* [2008].

[45] In this study, we compared electron features obtained by FAST at an altitude of ~ 3800 km with those by DS TC1 at $L = \sim 5.7$. Footprints of FAST and DS TC1 were mapped to similar latitudes and local times with differences of less than 5° and 1 h. We assumed that the electron acceleration or heating took place on a scale size larger than this difference of satellite footprints from the riometer data.

[46] From ~ 1352 UT, DS TC1 observed isotropic flux enhancements of electrons at energies above ~ 0.5 keV. The higher-energy electrons observed by DS TC1 appeared to be heated in the inner magnetosphere in association with the onset of a storm time substorm. The intense waves in the frequency range of 1–200 Hz associated with the electron flux enhancement may not contribute heating of the observed high-energy electrons, because such enhanced waves were only temporarily observed at ~ 1352 UT. The field fluctuations of the other frequency range or global change of the geomagnetic field configuration during the storm time substorm are likely to be the heating source of the higher-energy electrons.

[47] Based on magnetic field data obtained by FAST and DS TC1, it was found that field-aligned electrons at pitch angles less than $\sim 10^\circ$ at the DS TC1 altitude can reach the FAST altitude and extend to pitch angles between -90° and 90° by the mirror force. This result indicates a possibility that the field-aligned components at the DS TC1 altitude were observed as the isotropic higher-energy component of the BBES at the FAST altitude.

[48] The field-aligned electron fluxes were enhanced at energies of not only ~ 0.5 – 30 keV but also ~ 0.03 – 0.5 keV at FAST during the BBE event. The lower-energy field-aligned electrons below ~ 0.5 keV of BBES were not identified in the DS TC1 electron data. As a possible generation mechanisms for the field-aligned low-energy electrons, we speculate that they could be accelerated in field-aligned directions between the FAST and DS TC1 altitudes. A possible acceleration source for the lower-energy BBES is electron interaction with Alfvén waves. Chaston *et al.* [2002] simulated Alfvén wave propagation in the auroral oval to understand field and electron observations by FAST. In their study, the simulation successfully reproduced the observed electron distribution with an enhancement of parallel component over an energy range of 0.1–2 keV at altitudes where Alfvén wave electron acceleration occurs. Using FAST data, Mende *et al.* [2003] reported an event of intense field-aligned electron fluxes at suprathermal energies, which were probably accelerated by Alfvén waves, one minute after substorm onset. The intense field-aligned electron fluxes over energies of ~ 0.03 – 1 keV during the BBE event identified in our study are similar to the electron distributions reported by Chaston *et al.* [2002] and Mende *et al.* [2003]. The BBES were observed shortly after substorm onset, as in the case of Mende *et al.* [2003]. Alfvén waves generated during the substorm may contribute to the acceleration of the lower-energy BBES.

[49] Secondary electrons generated by precipitating electrons are the other possible source for the lower-energy BBES. Evans [1974] and Pulliam *et al.* [1981] showed that low-energy secondary electrons generated in the atmosphere can be backscattered by an upward field-aligned potential difference to form the low-energy part of auroral electron spectra. Evans [1974] showed that a majority of high-energy

electrons are isotropic and the backscattered low-energy electrons become field aligned. This point is consistent with the pitch angle features of the BBES. However, electron spectra do not always have monoenergetic peaks during BBE events (e.g., at 1356:43 UT in Figure 11), indicating that the field-aligned potential difference is probably not the cause of the BBES.

[50] The main generation mechanism for the lower-energy BBES may be an acceleration-like interaction with Alfvén waves. BBES possibly consist of two energy components due to acceleration or heating of electrons at different altitudes, as suggested by Nakajima *et al.* [2007].

4. Conclusion

[51] We studied the BBE event observed by FAST at 61°–66° ILATs, ~0600 MLT, and an altitude of ~3800 km at 1355–1359 UT during the main phase of a large storm on 25 July 2004. DS TC1 and GOES 10 were located at ~0600 MLT in the inner plasma sheet at $L = 5.7$ and 6.6, respectively. The observations and conclusions in this paper are summarized as follows.

[52] 1. GOES 10 observed the first signature of the expansion phase noting the onset of substorm as a dipolarization at ~1347 UT. Two minutes later, ground magnetic field data showed that positive and negative H-bays formed at ~1349 UT at ~0500–1000 MLTs. These facts indicate that substorms during the storm took place just before the BBE event. Perpendicular tailward ion flux was observed by DS TC1 at $L = 5.7$ from ~1350 UT for ~1 min. Then, DS TC1 observed a local dipolarization and ion density enhancement at ~1351 UT. The ion density enhancement lasted until after 1400 UT with isotropically enhanced electron and ion fluxes at energies above ~0.5 keV. We suggest that particle heating is occurring in the inner magnetosphere near DS TC1 associated with the onset of storm time substorm.

[53] 2. The footprints of FAST and DS TC1 were mapped to similar latitudes with differences of less than 5° and local time separation of ~1 h during the BBES. We compared electron features observed at different altitudes using FAST and DS TC1 data on the assumption that BBES were occurring over a spatial extent that included both of the satellite footprints. Electron flux enhancement at energies above ~0.5 keV from 1351 UT was observed by DS TC1. At FAST, electron fluxes were isotropic at higher energies above ~0.5 keV with an upward loss cone. On the other hand, at lower energies below ~0.5 keV, field-aligned electron fluxes were most intense. The field-aligned enhanced electrons at DS TC1 were probably observed as the isotropic higher-energy component of the BBES at FAST due to the mirror force. The field-aligned lower-energy component of the BBES at FAST might be accelerated in field-aligned directions through wave-particle interactions between the FAST and DS TC1 altitudes. From these results, we speculate that the BBES consist of the two-energy components due to acceleration or heating of electrons at different altitudes in association with the onset of storm time substorm.

[54] **Acknowledgments.** We thank Y. Asano at the Tokyo Institute of Technology for providing the PEACE data plot and helpful suggestions and T. Hori from Nagoya University for helpful discussions and suggestions.

We also acknowledge A. Runov from the Austrian Academy of Sciences (now at the University of California, Los Angeles) for helping us to use the PEACE data. The *Dst* index and geomagnetic field data were provided by the World Data Center-C2 for Geomagnetism, Kyoto University. We thank I. R. Mann for providing ground-based magnetic field data from the CANOPUS magnetometer array, now operated as CARISMA (<http://www.carisma.ca>) by the University of Alberta and funded by the Canadian Space Agency. Data were provided through the Canadian Space Science Data Portal (CSSDP, <http://www.cssdp.ca>). We acknowledge E. Donovan at the University of Calgary for providing riometer data through CSSDP. Conjunction Event Finder at DARTS JAXA/ISAS provided useful information for event selection. The package of subroutines and source code for calculation of satellite footprints was obtained from the Community Coordinated Modeling Center (CCMC), Goddard Space Flight Center. Solar wind and IMF data from ACE and magnetic field data from GOES 10 were provided by the coordinated data analysis web (CDAWeb) at NASA. This work was supported by the Grant-in-Aid for Scientific Research (A: 20244080, B: 18403011, 19403010, and 20340134), by the Dynamics of the Sun-Earth-Life Interactive System (G-4, the 21st Century COE program) from the Ministry of Education, Culture, Sports, Science, and Technology of Japan, and by a grant from the Research Fellowship from the Japan Society for the Promotion of Science.

[55] Amitava Bhattacharjee thanks the reviewers for their assistance in evaluating this paper.

References

- Baumjohann, W., G. Paschmann, and C. A. Cattell (1989), Average plasma properties in the central plasma sheet, *J. Geophys. Res.*, *94*, 6597–6606.
- Baumjohann, W., Y. Kamide, and R. Nakamura (1996), Substorms, storms, and the near-Earth tail, *J. Geomagn. Geoelectr.*, *48*, 177–185.
- Baumjohann, W., M. Hesse, S. Kokubun, T. Mukai, T. Nagai, and A. A. Petrukovich (1999), Substorm dipolarization and recovery, *J. Geophys. Res.*, *104*, 24,995–25,000.
- Bryant, D. A., D. S. Hall, and D. R. Lepine (1978), Electron acceleration in an array of auroral arcs, *Planet. Space Sci.*, *26*, 81–92.
- Carlson, C. W., R. F. Pfaff, and J. G. Watzin (1998), The Fast Auroral Snapshot (FAST) mission, *Geophys. Res. Lett.*, *25*, 2013–2016.
- Carlson, C. W., J. P. McFadden, P. Turin, D. W. Curtis, and A. Magoncelli (2001), The electrons and ion plasma experiment for FAST, *Space Sci. Rev.*, *98*, 33–66.
- Carr, C., et al. (2005), The Double Star magnetic field investigation: Instrument design, performance and highlights of the first year's observations, *Ann. Geophys.*, *23*, 2713–2732.
- Chaston, C. C., J. W. Bonnell, L. M. Peticolas, C. W. Carlson, J. P. McFadden, and R. E. Ergun (2002), Driven Alfvén waves and electron acceleration: A FAST case study, *Geophys. Res. Lett.*, *29*(11), 1535, doi:10.1029/2001GL013842.
- Cornilleau-Wehrlin, N., et al. (2005), The STAFF-DWP wave instrument on the DSP equatorial spacecraft: Description and first result, *Ann. Geophys.*, *23*, 2785–2801.
- Denig, W. F., and F. J. Rich (1986), The ionosphere-magnetosphere structure during a geomagnetic storm based on measurements in the morning auroral zone, *J. Geophys. Res.*, *91*, 165–182.
- Dombeck, J., C. Cattell, J. R. Wygant, A. Keiling, and J. Scudder (2005), Alfvén waves and Poynting flux observed simultaneously by Polar and FAST in the plasma sheet boundary layer, *J. Geophys. Res.*, *110*, A12S90, doi:10.1029/2005JA011269.
- Egeland, A., W. J. Burke, N. C. Maynard, E. M. Basinska, J. D. Winningham, and C. S. Deehr (1994), Ground and satellite observations of postdawn aurorae near the time of a sudden storm commencement, *J. Geophys. Res.*, *99*, 2095–2108.
- Elphic, R. C., J. D. Means, R. C. Snare, R. J. Strangeway, L. Kepko, and R. E. Ergun (2001), Magnetic field instruments for the Fast Auroral Snapshot explorer, *Space Sci. Rev.*, *98*, 151–168.
- Evans, D. S. (1974), Precipitating electron fluxes formed by a magnetic field aligned potential difference, *J. Geophys. Res.*, *79*, 2853–2858.
- Fazakerley, A. N., et al. (2005), The Double Star Plasma Electron and Current Experiment, *Ann. Geophys.*, *23*, 2733–2756.
- Frank, L. A., and K. L. Ackerson (1971), Observations of charged particle precipitation into the auroral zone, *J. Geophys. Res.*, *76*, 3612–3643.
- Liu, Z. X., C. P. Escoubet, Z. Pu, H. Laakso, J. K. Shi, C. Shen, and M. Hapgood (2005), The Double Star mission, *Ann. Geophys.*, *23*, 2707–2712.
- Lui, A. T. Y., D. Venkatesan, C. D. Anger, S.-I. Akasofu, W. J. Heikkilä, J. D. Winningham, and J. R. Burrows (1977), Simultaneous observations of particle precipitations and auroral emissions by the ISIS 2 satellite in the 19–24 MLT sector, *J. Geophys. Res.*, *82*, 2210–2226.

- McEwen, D. J., C. N. Duncan, and R. Montalbetti (1981), Auroral electron energies: Comparisons of in situ measurements with spectroscopically inferred energies, *Can. J. Phys.*, *59*, 1116–1123.
- Mende, S. B., C. W. Carlson, H. U. Fray, L. M. Peticolas, and N. Stgaard (2003), FAST and IMAGE-FUV observations of a substorm onset, *J. Geophys. Res.*, *108*(A9), 1344, doi:10.1029/2002JA009787.
- Miyashita, Y., S. Machida, T. Mukai, Y. Saito, K. Tsuruda, H. Hayakawa, and P. R. Sutcliffe (2000), A statistical study of variations in the near and midlatitude magnetotail associated with substorm onsets: Geotail observations, *J. Geophys. Res.*, *105*, 15,913–15,930.
- Miyashita, Y., S. Machida, K. Liou, T. Mukai, Y. Saito, H. Hayakawa, C.-I. Meng, and G. K. Parks (2003), Evolution of the magnetotail associated with substorm auroral breakups, *J. Geophys. Res.*, *108*(A9), 1353, doi:10.1029/2003JA009939.
- Miyashita, Y., et al. (2005), Geotail observations of signatures in the near-Earth magnetotail for the extremely intense substorms of the 30 October 2003 storm, *J. Geophys. Res.*, *110*, A09S25, doi:10.1029/2005JA011070.
- Nagai, T., M. Fujimoto, Y. Saito, S. Machida, T. Terasawa, R. Nakamura, T. Yamamoto, T. Mukai, A. Nishida, and S. Kokubun (1998), Structure and dynamics of magnetic reconnection for substorm onsets with Geotail observations, *J. Geophys. Res.*, *103*, 4419–4440.
- Nakajima, A., K. Shiokawa, K. Seki, R. J. Strangeway, J. P. McFadden, and C. W. Carlson (2007), Particle and field characteristics of broadband electrons observed by the FAST satellite during a geomagnetic storm, *J. Geophys. Res.*, *112*, A06220, doi:10.1029/2006JA012184.
- Nakajima, A., K. Shiokawa, K. Seki, J. P. McFadden, C. W. Carlson, R. J. Strangeway, and K. Yumoto (2008), Particle and field characteristics of broadband electrons observed by the FAST satellite during geomagnetic storms: A multievent study, *J. Geophys. Res.*, *113*, A06221, doi:10.1029/2007JA013001.
- Ohtani, S., A. T. Y. Lui, K. Takahashi, D. G. Mitchell, and T. Sarris (2000), Ion dynamics and tail current intensification prior to dipolarization: The June 1, 1985, event, *J. Geophys. Res.*, *105*, 25,233–25,246.
- Pulliam, D. M., H. R. Anderson, K. Stamnes, and M. H. Rees (1981), Auroral electron acceleration and atmospheric interactions: (1) Rocket-borne observations and (2) scattering calculations, *J. Geophys. Res.*, *86*, 2397–2404.
- Rème, H., et al. (2005), The HIA instrument on board the Tan Ce 1 Double Star near-equatorial spacecraft and its first results, *Ann. Geophys.*, *23*, 2757–2774.
- Schödel, R., K. Diershke, W. Baumjohann, R. Nakamura, and T. Mukai (2002), The storm time central plasma sheet, *Ann. Geophys.*, *20*, 1737–1741.
- Sharber, J. R., R. A. Frahm, R. Link, G. Crowley, J. D. Winningham, E. E. Gaines, R. W. Nightingale, D. L. Chenette, B. J. Anderson, and C. A. Gurgiolo (1998), UARS particle environment monitor observations during the November 1993 storm: Auroral morphology, spectral characterization, and energy deposition, *J. Geophys. Res.*, *103*, 26,307–26,322.
- Shiokawa, K., K. Yumoto, C.-I. Meng, and G. Reeves (1996), Broadband electrons observed by the DMSP satellites during storm time substorms, *Geophys. Res. Lett.*, *23*, 2529–2532.
- Shiokawa, K., C.-I. Meng, G. D. Reeves, F. J. Rich, and K. Yumoto (1997), A multievent study of broadband electrons observed by the DMSP satellites and their relation to red aurora observed at midlatitude stations, *J. Geophys. Res.*, *102*, 14,237–14,253.
- Shiokawa, K., R. R. Anderson, I. A. Daglis, W. J. Hughes, and J. R. Wygant (1999), Simultaneous DMSP and CRRES observation of broadband electrons during a storm-time substorm on March 25, 1991, *Phys. Chem. Earth*, *24*, 281–285.
- Takada, T., R. Nakamura, W. Baumjohann, Y. Asano, M. Volwerk, T. L. Zhang, B. Klecker, H. Rème, E. A. Lucek, and C. Carr (2006), Do BBFs contribute to inner magnetosphere dipolarizations: Concurrent Cluster and Double Star observations, *Geophys. Res. Lett.*, *33*, L21109, doi:10.1029/2006GL027440.
- Tsyganenko, N. A. (1995), Modeling the Earth's magnetospheric magnetic field confined within a realistic magnetopause, *J. Geophys. Res.*, *100*, 5599–5612.
- Tsyganenko, N. A. (1996), Effects of the solar wind conditions on the global magnetospheric configuration as deduced from data-based field models, in *Third International Conference on Substorms (ICS-3), Versailles, France, 12–17 May 1996*, edited by E. Rolfe and B. Kaldeich, *Eur. Space Agency Spec. Publ., ESA SP-389*, 181–185.
- W. Baumjohann and R. Nakamura, Space Research Institute, Austrian Academy of Sciences, Schmiedlstr. 6, A-8042 Graz, Austria. (baumjohann@oeaw.ac.at; rumi@oeaw.ac.at)
- C. W. Carlson and J. P. McFadden, Space Sciences Laboratory, University of California, 7 Gauss Way, Berkeley, CA 94720-7450, USA. (cwc@apollo.ssl.berkeley.edu; mcfadden@apollo.ssl.berkeley.edu)
- N. Cornilleau-Wehrin and O. Le Contel, Laboratoire de Physique des Plasmas, Ecole Polytechnique, UPMC, CNRS, F-91128 Palaiseau CEDEX, France. (nicole.cornilleau@lpp.polytechnique.fr; olivier.lecontel@lpp.polytechnique.fr)
- I. Dandouras and H. Rème, Centre d'Etude Spatiale des Rayonnements, Toulouse University, CNRS, BP 44346, 9 Ave. du Colonel Roche, F-31028 Toulouse CEDEX, France. (iannis.dandouras@cesr.fr; henri.reme@cesr.fr)
- A. N. Fazakerley, Mullard Space Science Laboratory, University College London, Dorking RH5 6NT, UK. (anf@mssl.ucl.ac.uk)
- K. Keika, Center for Solar-Terrestrial Research, New Jersey Institute of Technology, 323 Martin Luther King Jr. Blvd., Newark, NJ 07102-1982, USA. (keika@adm.njit.edu)
- A. Nakajima, K. Seki, and K. Shiokawa, Solar-Terrestrial Environment Laboratory, Nagoya University, Furo-cho, Chikusa-ku, Nagoya, Aichi 464-8601, Japan. (akimitsu@stelab.nagoya-u.ac.jp; seki@stelab.nagoya-u.ac.jp; shiokawa@stelab.nagoya-u.ac.jp)
- R. J. Strangeway, Institute of Geophysics and Planetary Physics, University of California, 405 Hilgard Ave., Los Angeles, CA 90024-1567, USA. (strange@igpp.ucla.edu)
- T. Takada, Institute of Space and Astronautical Science, JAXA, Yoshinodai 3-1-1, Sagami-hara, Kanagawa 229-8510, Japan. (takada@stp.isas.jaxa.jp)
- K. H. Yearby, Department of ACSE, University of Sheffield, Mappin Street, Sheffield S1 3JD, UK. (h.h.yearby@sheffield.ac.uk)